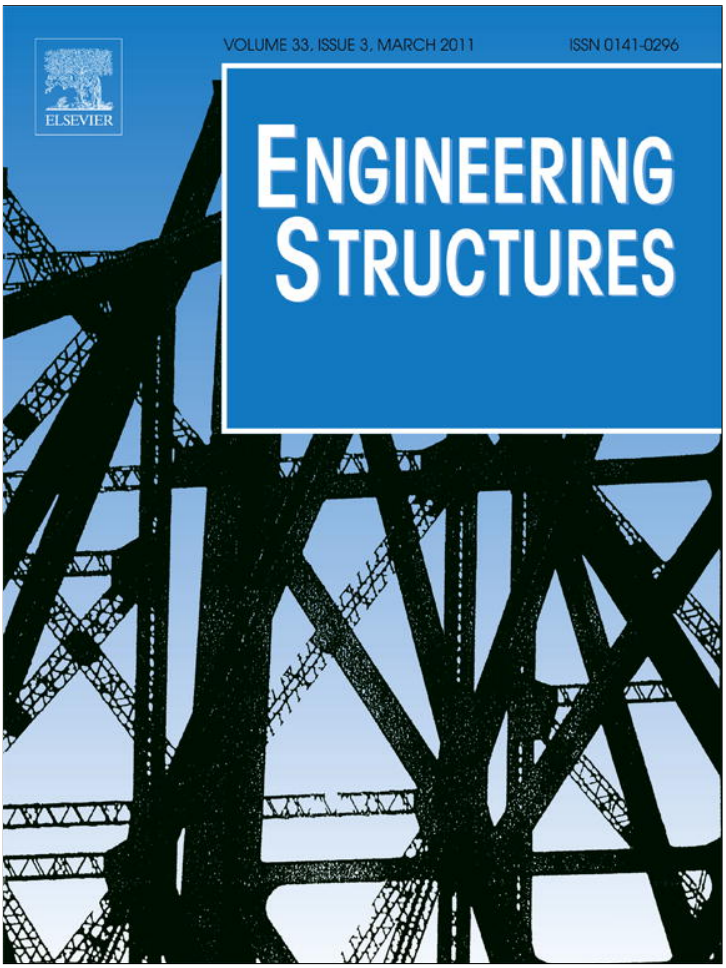

Engineering Structures 33 (2011) 813–826

Contents lists available at ScienceDirect

Engineering Structures

journal homepage: www.elsevier.com/locate/engstruct

Seismic response analysis of skew bridges with pounding deck–abutment joints

Elias G. Dimitrakopoulos

Department of Engineering, University of Cambridge, CB2 1PZ, United Kingdom

ARTICLE INFO

Article history:
Received 19 May 2010
Received in revised form
11 November 2010
Accepted 1 December 2010
Available online 8 January 2011

Keywords:
Skew bridges
Unilateral contact
Non-smooth structural dynamics
Concrete bridges

ABSTRACT

In this paper the seismic response of short skew bridges with deck–abutment pounding joints is revisited. The permanent deck rotations and transverse displacements of such bridges after the recent earthquake in Chile created an incentive to revisit their non-conventional behaviour. A novel non-smooth rigid body approach is proposed to analyze the seismic response of pounding skew bridges which involves oblique frictional multi-contact phenomena. The coupling of the response, due to contact, is analysed in depth. It is shown that the tendency of skew bridges to exhibit transverse displacements and/or rotate (and hence unseat) after deck–abutment collisions is not a factor of the skew angle alone, but rather of the plan geometry plus friction. This is expressed with proposed dimensionless criteria. The study also unveils that the coupling is more pronounced in the low range of the frequency spectrum (short-period excitations/flexible structures) and presents novel dimensionless response spectra for the transverse displacements and rotations, triggered by oblique contact in a skew bridge subsystem. Despite the complexity of the response, the proposed spectra highlight a clear pattern. The dimensionless rotations, arising from contact, decline as the ratio of the structural versus excitation frequency increases and become practically negligible in the upper range of the frequency spectrum. Finally, a pilot application to a typical skew bridge is presented.

1. Introduction

This paper focuses on the seismic response of short skew bridges with deck–abutment joints, while it derives from a broader study [1–4] on the problem of earthquake-induced pounding in bridges. The recent earthquake in Chile [5,6] has created an incentive to revisit the non-conventional behaviour of skew bridges. As earthquake reconnaissance reports [7] indicate, skew bridges often rotate in the horizontal plane, thus tending to drop off the supports at the acute corners [8]. This behaviour is triggered by oblique contact and results in coupling of longitudinal and transverse response, binding in one of the obtuse corners and subsequently rotation in the direction of increasing the skew angle [8] (see also Fig. 1). Despite the recorded evidence from previous earthquakes which underline the importance of this mechanism, as well as the empirical vulnerability methodologies that acknowledge skew as a primary vulnerability factor of bridges [9], there are only a few analytical attempts to comprehend this mechanism.

One of the first contributions was made by Maragakis et al. [10], motivated by extensive damage during the 1971 San Fernando [7] earthquake. Maragakis et al. [10] focused on the interaction of short skew bridges with the abutments and the resulting rigid body rotational vibrations. In that study, the bridge deck was simulated with a rigid stick model and pounding with the abutments was taken into account with a spring activated after the gap closure. The analysis performed therein showed significant transverse displacements at the end supports due to rotations. Planar rigid body deck rotations were found to be primarily produced by impact of the skew deck with the abutment and not by non-symmetric (e.g. eccentricity in plan with respect to the centre of mass) restoring characteristics of the substructure, or impact between deck and wing walls. More than 20 years later, Abdel-Mohti and Pekcan [11] compared detailed 3D finite element modelling with simplified beam stick models of skew bridges and argued that the beam stick model is capable of capturing the coupling of the response and the main modes of the bridge, at least for moderate skew angles.

In their recent study, Saadeghvaziri and Yardani-Motlagh [12] examined the seismic vulnerability of Multi-Span Simply-Supported (MSSS) bridges. They marked that impact can impose high shear demands on the bearings of MSSS skew bridges, raising their failure probability. The coupling of the response displacements as well as rotations, caused by skew deck–abutment contact, was also underlined by Bignell et al. [13]. Bignell et al. conducted a series of push-over analyses with structural configurations representative of typical Illinois bridges. The ultimate load capacity of a bridge was reduced, due to the skew angle, up to nearly two thirds compared to the corresponding non-skew bridge. In addition, the presence of a skew angle introduced failure mechanisms unseen in the non-skew case, e.g. abutment bearing failure. Maleki [14] studied single span skew bridges using a SDOF model in an attempt to

E-mail address: ilias.dimitrakopoulos@gmail.com.

0141-0296/$ – see front matter © 2010 Elsevier Ltd. All rights reserved.
doi:10.1016/j.engstruct.2010.12.004

Notations

α	skew angle (as defined in Fig. 2)
a_g, ω_g	a length and a time scale of the excitation appropriately selected as in [3]
$\ddot{u}_g$	ground acceleration, upper dots stand for differentiation with respect to time.
W, L	Width, Length of a bridge deck in plan (as defined in Fig. 2)
δ	gap size at rest
η_0, η_1	dimensionless skew ratio for frictionless and frictional contact respectively, defined in Eq. (1)
Λ_{Ni}, Λ_{Ti}	impulse in the normal and the tangential direction of contact i respectively
$\mathbf{\Lambda}_N$, $\mathbf{\Lambda}_T$	the column vector of impulses Λ_{Ni} and Λ_{Ti} respectively
$\boldsymbol{\lambda}$, $\boldsymbol{\lambda}_N$, $\boldsymbol{\lambda}_T$, $\boldsymbol{\lambda}_H$	vector of the contact force, in the normal direction (subscript 'N') and the tangential direction for sliding (subscript 'T') and sticking (subscript 'H') contacts.
r_i	lever arms in the normal direction of contact i (Eqs. (8))
r_T	lever arms in the tangential direction of contact i, $r_T = Lc\alpha/2$
ω_0, ω_{0x}, ω_{0y}	translational angular frequency, subscripts 'x' and 'y' indicate the translational direction when is needed
Ω_0	rotational angular frequency
ξ	viscous damping ratio
x, x_m	translational displacement in x–x direction, subscript 'm' stands for maximum
y, y_m	translational displacement in y–y direction, subscript 'm' stands for maximum
θ, θ_m	planar rotation around the vertical axis, subscript 'm' stands for maximum
$\mathbf{q}$	vector of the relative to the ground displacements, $\mathbf{q}^T = (x\ y\ \theta)$
$\mathbf{u}$	vector of the relative to the ground velocities ($\dot{\mathbf{q}} = \mathbf{u}$ holds almost everywhere)
T_m	mean period. $T_m = \sum_i \left(C_i^2/f_i\right) / \sum_i C_i^2$ where C_i are the Fourier amplitudes of the accelerogram and f_i the discrete Fourier transform frequencies between 0.25 and 20 Hz.
$\mathbf{h}$	vector of the non-impulsive forces
m, I_m, $\mathbf{M}$	mass, rotational moment of inertia and mass matrix respectively
ρ	radius of gyration
$\mathbf{E}$	identity matrix
ε_{Ni}, $\bar{\bar{\varepsilon}}_N$	coefficient of restitution in the normal direction of contact i and diagonal matrix: $\bar{\bar{\varepsilon}}_N = \text{diag}\{\varepsilon_{Ni}\}$
μ_i, $\bar{\bar{\boldsymbol{\mu}}}$	coefficient of friction of contact point i and diagonal matrix: $\bar{\bar{\boldsymbol{\mu}}} = \text{diag}\{\mu_i\}$
$\bar{\bar{\boldsymbol{\mu}}}_G$, $\bar{\bar{\boldsymbol{\mu}}}_H$	the $\bar{\bar{\boldsymbol{\mu}}}$ matrices for sliding (subscript 'T') and sticking contacts (subscript 'H')
g_{Ni}	relative distance of the potential contact i
γ_{Ni}, γ_{Ti}	the velocities of contact i in the normal and the tangential direction of respectively
$\boldsymbol{\gamma}_N$, $\boldsymbol{\gamma}_T$	vector of contact velocities γ_{Ni} and γ_{Ti}
$\boldsymbol{\gamma}_{NA}$, $\boldsymbol{\gamma}_{NE}$	the contact velocities vector before (subscript 'A') and after (subscript 'E') contact in the normal direction
$\boldsymbol{\gamma}_{TA}$	the tangential contact velocity vector before
$\boldsymbol{\gamma}_{TE} = \boldsymbol{\gamma}_{TR} - \boldsymbol{\gamma}_{TL}$	the tangential post-contact velocity vector, which is decomposed into the positive (subscript 'R') and negative (subscript 'L') part
$\dot{\boldsymbol{\gamma}}_H = \dot{\boldsymbol{\gamma}}_{HR} - \dot{\boldsymbol{\gamma}}_{HL}$	the tangential contact acceleration vector of the sticking contacts, which is decomposed into the positive (subscript 'R') and negative (subscript 'L') part
$\mathbf{W}_N$, $\mathbf{W}_T$	direction matrices in the normal (subscript 'N') and the tangential (subscript 'T') direction of contacts
$\mathbf{W}_H$, $\mathbf{W}_G$	direction matrices of the potentially sticking contacts (subscript 'H') and sliding contacts (subscript 'G')
$\mathbf{W}_Q$	the abbreviation $\mathbf{W}_Q = \mathbf{W}_N + \mathbf{W}_G\bar{\bar{\boldsymbol{\mu}}}_G + \mathbf{W}_T\bar{\bar{\boldsymbol{\mu}}}_T$
$()^T$	denotes the transpose matrix
3D	Three Dimensional
C.M.	Centre of Mass
MSSS	Multi-Span Simply-Supported
PGA	Peak Ground Acceleration
SDOF	Single Degree of Freedom
MDOF	Multi Degree of Freedom
LCP	Linear Complementarity Problem

Fig. 1. Typical damage of overcrossings after the Chile earthquake of February 27, 2010.
Source: Taken from [5].

estimate the forces developed during collision. Lou and Zerva [15] emphasized the need for more realistic spatially variable ground motions when analysing the seismic response of a skew bridge with deck–abutment joints.

Meng et al. [16,17] examined the torsional effects introduced in short skew bridges by (accidental or other) eccentricity but did not consider deck–abutment contact. The most relevant conclusion of these studies [18,16], to the present work, is that the rotation of skew bridges with high rotational Ω_0 to translational ω_0 frequency ratios (Ω_0/ω_0) may be less sensitive to the deck-aspect ratio Width/Length $= W/L$ and the skew angle α (Fig. 2).

Some of the salient features of the rotational mechanism associated with the deck–abutment collisions of skew bridges were brought forward in [2]. Studying the oblique impact of a planar skew rigid body against an inelastic half-space (Fig. 2), that study revealed that what matters during full-edge impact is the total geometry of the (skew) deck in plan. In particular the dimensionless skew ratio η_0 and η_1 for frictionless and frictional impact respectively are important:

$$\eta_0 = \frac{\sin 2\alpha}{2\,(W/L)}, \qquad \eta_1 = \eta_0\left(1 + \frac{\mu}{\tan\alpha}\right) \tag{1}$$

When $\eta_0 < 1$ (Fig. 2-top) the angular momentums $r_1\Lambda_{N1}$ and $r_2\Lambda_{N2}$ of the two impulses Λ_{N1} and Λ_{N2} are in different directions

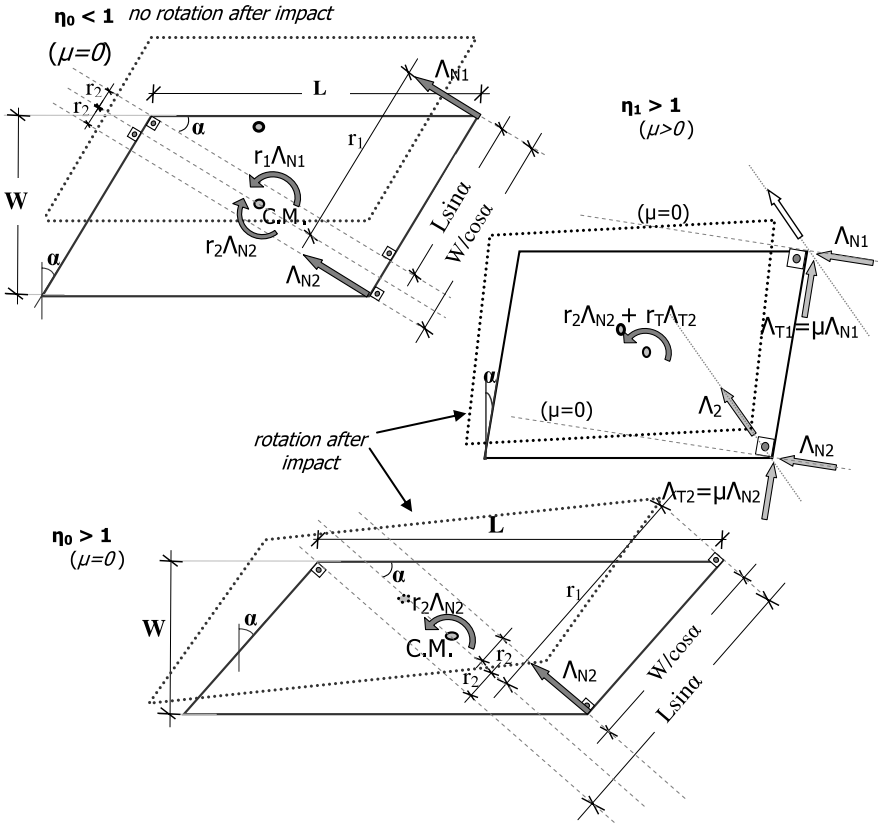

Fig. 2. Geometrical interpretation (plan view) of the rotational mechanism triggered by deck–abutment impact in skew bridges. Top: no rotation is developed after full-edge frictionless impact. Bottom: full-edge frictionless impact results in rotation. Middle: frictional full-edge impact results in rotation when the resultant impulses are in the same direction with respect to the centre of mass.

with respect to the centre of mass (C.M.) and cancel out. Consequently, no angular velocity and hence rotation is developed; a non-intuitive behaviour [2]. On the contrary, when $\eta_0 > 1$ (Fig. 2 bottom) the angular momentums of the two impulses are in the same direction, contact at the acute corner is lost [2] and angular velocity is developed. The same principle applies for the more complex case of frictional collisions [2]; frictional impact (Fig. 2-middle) leads to rotation when the angular momentums of the two impulses are in the same direction with respect to the C.M. ($\eta_1 > 1$).

The motivation for this study originates from (i) the increased vulnerability of skew bridges acknowledged by most empirical vulnerability methodologies (ii) the need to elucidate the seismic response of skew bridges with (deck–abutment) joints and (iii) the large number of such existing bridges worldwide. The scope of the present paper is to examine how the geometry of the deck alters frictionless or frictional, deck–abutment, contact and thus, the seismic behaviour of skew bridges. The main contributions of this study are on one hand, the novel non-smooth dynamics approach of analysing the seismic response and on the other hand, the use of formal dimensional analysis for describing the response of pounding skew bridges.

2. Proposed approach

2.1. Non-smooth dynamics

The dynamic response of skew bridges with joints is revisited with a non-smooth dynamics methodology which is event-based [19] and originates from multibody dynamics with unilateral contacts [20]. A key feature of an event-based methodology is the decomposition of the non-smooth response, such as the dynamic response of pounding bridge segments (see also [1]), into discontinuous events (e.g. impacts and contacts) and continuous impact-free motion [21]. Unlike many relevant studies which adopt a contact element (compliance) approach, unilateral contact [4] is used to describe the interaction between the (skew) deck and the abutment. The bridge deck, in between the deck–abutment expansion joints, is considered as a planar rigid body.

The equation of motion of a multibody system with unilateral contacts can be written as [20]:

$$\mathbf{M}(t, \mathbf{q})\dot{\mathbf{u}} - \mathbf{h}(t, q, u, \ddot{u}_g) - \mathbf{W}_N \boldsymbol{\lambda}_N - \mathbf{W}_T \boldsymbol{\lambda}_T = 0 \tag{2}$$

where $\mathbf{M}$ is the mass matrix and $\mathbf{W}_N$ and $\mathbf{W}_T$ are the direction matrices of the constraints (contacts) in the normal (subscript 'N') and the tangential (subscript 'T') direction (N, T are used throughout this paper in the same sense), $\mathbf{q}$ is the vector of the relative to the ground displacements, $\mathbf{u}$ the corresponding velocities for which $\dot{\mathbf{q}} = \mathbf{u}$ holds almost everywhere, $\ddot{u}_g$ the ground acceleration, $\mathbf{h}$ the vector of the non-impulsive forces and $\boldsymbol{\lambda}$ is the contact force vector which can be considered as a Lagrange multiplier (see also [19]).

Herein, the most fundamental (and well-known) impact laws are adopted in a set-valued form according to [2]. Impact is assumed to behave according to Newton's law in the normal direction and according to Coulomb's friction law in the tangential direction. Hence, only two impact parameters are needed to describe frictional impact, the normal coefficient of restitution ε_N and the coefficient of friction μ. The Newton's coefficient of restitution is taken as the ratio of the (relative) contact velocities after γ_{NE}, and before γ_{NA}, impact: $\gamma_{NE} = -\varepsilon_N \gamma_{NA}$ (subscript 'E' denotes the expansion phase and subscript 'A' the approach phase of impact). The coefficient of restitution varies between zero and one in the normal direction, and is assumed to be zero in the tangential direction in order to realize Coulomb's friction law.

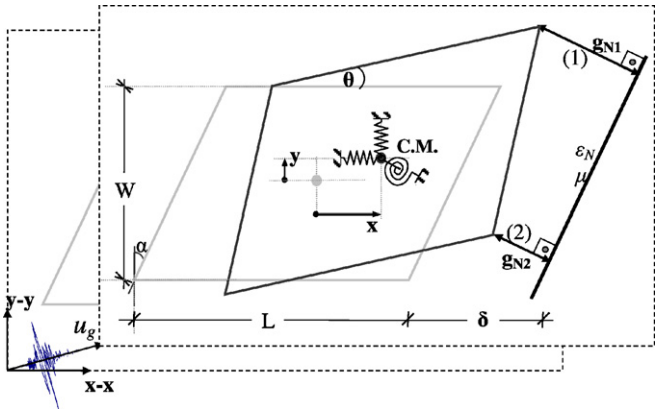

Fig. 3. Relative distance of the two potential contacts g_{N1} and g_{N2} for planar motion of a skew bridge deck segment (rigid body). Grey line—initial position, black line—position after translational and rotational motion. The system (in the grey frame) is subjected to ground motion u_g.

According to the adopted approach, the (multi-point and oblique) contact of skew bridges with joints is formulated as a Linear Complementarity Problem (LCP). In the classical form, an LCP is a system of linear equations (e.g. Eq. (3) later on) for which additional complementarity conditions hold (Eqs. (4)) [22]. Lemke's pivotal algorithm [22] is employed to solve the LCP numerically.

Impacts:

The velocity jumps associated with impacts are captured with a LCP formulated on the velocity level, presented in detail in [2]. By defining $\boldsymbol{\gamma}_N = \mathbf{W}_N^T\mathbf{u}$ and $\boldsymbol{\gamma}_T = \mathbf{W}_T^T\mathbf{u}$ as the vectors of the contact velocities in the normal and the tangential direction of contact respectively, and the pertinent impulse vectors with $\boldsymbol{\Lambda}_\mathbf{N}$ and $\boldsymbol{\Lambda}_\mathbf{T}$, an LCP is formulated that treats a frictional multi-impact:

$$\begin{pmatrix} \gamma_{NE} + \bar{\bar{\varepsilon}}_N\gamma_{NA} \\ \gamma_{TR} \\ \bar{\bar{\mu}}\Lambda_N - \Lambda_T \end{pmatrix} = \begin{pmatrix} W_N^TM^{-1}\left(W_N - W_T\bar{\bar{\mu}}\right) & W_N^TM^{-1}W_T & 0 \\ W_T^TM^{-1}\left(W_N - W_T\bar{\bar{\mu}}\right) & W_T^TM^{-1}W_T & E \\ 2\bar{\bar{\mu}} & -E & 0 \end{pmatrix} \times \begin{pmatrix} \Lambda_N \\ \bar{\bar{\mu}}\Lambda_N + \Lambda_T \\ \gamma_{TL} \end{pmatrix} + \begin{pmatrix} \left(\bar{\bar{\varepsilon}}_N + E\right)\gamma_{NA} \\ E\gamma_{TA} \\ 0 \end{pmatrix} \tag{3}$$

$$\begin{pmatrix} \gamma_{NE} + \bar{\bar{\varepsilon}}_N\gamma_{NA} \\ \gamma_{TR} \\ \bar{\bar{\mu}}\Lambda_N - \Lambda_T \end{pmatrix} \geq 0, \qquad \begin{pmatrix} \Lambda_N \\ \bar{\bar{\mu}}\Lambda_N + \Lambda_T \\ \gamma_{TL} \end{pmatrix} \geq 0,$$

$$\begin{pmatrix} \gamma_{NE} + \bar{\bar{\varepsilon}}_N\gamma_{NA} \\ \gamma_{TR} \\ \bar{\bar{\mu}}\Lambda_N - \Lambda_T \end{pmatrix}^T \begin{pmatrix} \Lambda_N \\ \bar{\bar{\mu}}\Lambda_N + \Lambda_T \\ \gamma_{TL} \end{pmatrix} = 0 \tag{4}$$

where: γ_{TR}, γ_{TL} are the positive and negative parts of the tangential post-impact velocity (see also [2]), γ_{TA} is the tangential pre-impact velocity, $\mathbf{E}$ is the identity matrix, $\bar{\mu} = \text{diag}\{\mu_i\}$ and $\bar{\varepsilon}_N = \text{diag}\{\varepsilon_{Ni}\}$, with i being the index of the impact points.

The LCP described by Eqs. (3) and (4) yields a great variety of solutions and is capable of encapsulating different impact states such as "slip", "stick" and reversal of sign, both for single and for double impact [2].

Continuous contact and detachment:

Unlike the LCP dealing with the impacts which is formulated on the velocity level, the LCP for continuous contacts and detachment (not considered in [2]) is formulated on the acceleration level. Let $\dot{\gamma}_N$ and λ_N be the acceleration and force vectors (in the normal direction) of the active contacts, $\dot{\gamma}_{HR}$ and $\dot{\gamma}_{HL}$ the positive and negative parts of the tangential acceleration vector respectively, and λ_H the pertinent force vector of the potentially sticking contacts (subscript 'H'). Then the associated LCP can be written as [19]:

$$\begin{pmatrix} \dot{\gamma}_N \\ \dot{\gamma}_{HL} \\ \bar{\bar{\mu}}_H\lambda_N + \lambda_H \end{pmatrix} = \begin{pmatrix} W_N^TM^{-1}W_Q & -W_N^TM^{-1}W_H & 0 \\ -W_H^TM^{-1}W_Q & W_H^TM^{-1}W_H & E \\ 2\bar{\bar{\mu}}_H & -E & 0 \end{pmatrix} \times \begin{pmatrix} \lambda_N \\ \bar{\bar{\mu}}_H\lambda_N - \lambda_H \\ \dot{\gamma}_{HR} \end{pmatrix} + \begin{pmatrix} W_N^TM^{-1}h \\ -W_N^TM^{-1}h \\ 0 \end{pmatrix} \tag{5}$$

$$\begin{pmatrix} \dot{\gamma}_N \\ \dot{\gamma}_{HL} \\ \bar{\bar{\mu}}_H\lambda_N + \lambda_H \end{pmatrix} \geq 0, \qquad \begin{pmatrix} \lambda_N \\ \bar{\bar{\mu}}_H\lambda_N - \lambda_H \\ \dot{\gamma}_{HR} \end{pmatrix} \geq 0,$$

$$\begin{pmatrix} \dot{\gamma}_N \\ \dot{\gamma}_{HL} \\ \bar{\bar{\mu}}_H\lambda_N + \lambda_H \end{pmatrix}^T \begin{pmatrix} \lambda_N \\ \bar{\bar{\mu}}_H\lambda_N - \lambda_H \\ \dot{\gamma}_{HR} \end{pmatrix} = 0 \tag{6}$$

where: W_H, W_G are the direction matrices and $\bar{\bar{\mu}}_H$, $\bar{\bar{\mu}}_G$ the diagonal matrices with the coefficients of friction of the potentially sticking contacts (subscript 'H') and sliding contacts (subscript 'G') and W_Q the abbreviation: $W_Q = W_N + W_G\bar{\bar{\mu}}_G + W_H\bar{\bar{\mu}}_H$.

Contact kinematics of skew bridges with deck–abutment joints:

Fig. 3 presents a skew bridge segment (rigid body) moving in plan against an inelastic half-space. The system is excited by a ground motion u_g. The generalised coordinates vector can be considered as the three degrees of freedom of a planar rigid body relative to the ground: $\mathbf{q}^T = (x\ y\ \theta)$, where x, y are the two translational DOF along the two horizontal axes and one rotational θ around the vertical axis (Fig. 3).

The relative distance of the two potential contacts g_{N1}, g_{N2} (gap functions) can be derived, using trigonometry as [2,23]:

$$\begin{aligned} g_{N1} &= (\delta - x)\,c\alpha + ys\alpha + \frac{1}{2}\left[Lc\alpha(1 - \cos\theta) + 2r_1\sin\theta\right] \\ g_{N2} &= (\delta - x)\,c\alpha + ys\alpha - \frac{1}{2}\left[Lc\alpha\,(\cos\theta - 1) + 2r_2\sin\theta\right] \end{aligned} \tag{7}$$

where δ is the gap size, α the skew angle, L the length and W the width of the rigid body respectively, and the following notations are used:

$$\begin{aligned} &c\alpha = \cos\alpha, \qquad s\alpha = \sin\alpha, \qquad r_1 = (Ls\alpha + W/c\alpha)/2, \\ &r_2 = (Ls\alpha - W/c\alpha)/2. \end{aligned} \tag{8}$$

Quantities r_1, r_2 are the corresponding lever arms in the normal direction and $r_T = Lc\alpha/2$ (used in Eqs. (9)) in the tangential direction of the two contact points, for small rotations. The relative velocities of the two impacts in the normal γ_{N1} and γ_{N2} and the tangential direction γ_{T1} and γ_{T2}, are given by [2]:

$$\begin{aligned} \gamma_{Ni} &= \underbrace{\begin{pmatrix} -c\alpha & s\alpha & \frac{1}{2}\left[Lc\alpha\sin\theta + 2r_i\cos\theta\right] \end{pmatrix}}_{W_{Ni}^T} \underbrace{\begin{pmatrix} \dot{x} \\ \dot{y} \\ \dot{\theta} \end{pmatrix}}_{u} \\ \gamma_{Ti} &= \underbrace{\begin{pmatrix} s\alpha & c\alpha & \frac{1}{2}\left[-2r_i\sin\theta + 2r_T\cos\theta\right] \end{pmatrix}}_{W_{Ti}^T} \underbrace{\begin{pmatrix} \dot{x} \\ \dot{y} \\ \dot{\theta} \end{pmatrix}}_{u}, \\ &i = 1, 2. \end{aligned} \tag{9}$$

2.2. Dimensional analysis

In order to present the results of the subsequent analysis in a way that is condensed and meaningful for a wide range of bridge configurations, dimensional analysis is implemented. The application of the proposed method hinges upon a distinct

length scale (a_g) and a time scale (ω_g) that characterise the ground shaking. In records with distinct pulses, the acceleration amplitude and duration of the pulse are usually selected (see [1] and references therein), while for records without distinct pulses the peak ground acceleration ($a_g = PGA$) and the mean period T_m [24] ($\omega_g = 2\pi/T_m$) can be used [3]. $T_m = \sum_i \left(C_i^2/f_i\right) / \sum_i C_i^2$, where C_i are the Fourier amplitudes of the accelerogram and f_i the discrete Fourier transform frequencies between 0.25 and 20 Hz.

With reference to Fig. 3, the parameters that determine the response of the simplest mechanical configuration of a skew bridge are the:

- (elastic) dynamic characteristics of the system: the angular frequency and the damping ratio of the translational (ω_0, ξ) and the rotational (Ω_0, ξ) degrees of freedom accordingly.
- contact parameters: coefficient of restitution, ε_N and coefficient of friction μ.
- geometrical characteristics: length L, width W, skew angle α and gap size at rest δ.
- characteristics of the excitation, acceleration amplitude a_g and angular frequency ω_g appropriately selected as in [3].

The response quantities can thus be written as a function of the general form:

$$\theta_m, x_m, y_m = f\left(\omega_0, \Omega_0, \xi, \delta, \varepsilon_N, \mu, W, L, \alpha, a_g, \omega_g\right). \tag{10}$$

The response function is thus governed by 1 independent (e.g. maximum displacement along the x–x axis x_m, maximum displacement along the y–y axis y_m or maximum rotation θ_m) and 11 dependent variables which involve only 2 reference dimensions, those of length [L] and time [T]. According to Buckingham's "Π" theorem [25,26], the number of independent dimensionless Π-products is now: (12 variables) – (2 reference dimensions) = 10Π-terms.

Here the following dimensionless form is proposed for the response function:

$$\frac{\theta_m \rho \omega_g^2}{a_g}, \frac{x_m \omega_g^2}{a_g}, \frac{y_m \omega_g^2}{a_g} = \Phi\left(\frac{\omega_0}{\omega_g}, \frac{\omega_0}{\Omega_0}, \xi, \frac{\delta \omega_g^2}{a_g}, \varepsilon_N, \mu, \frac{W}{L}, \frac{\delta}{L}, \alpha\right). \tag{11}$$

The novel proposition of the present paper is the dimensionless rotation term $\theta_m \rho \omega_g^2/a_g$. The maximum response rotation θ_m, arising from oblique contact, is normalized by both the persistence of the excitation a_g/ω_g^2 and to the radius of gyration ρ ($\rho^2 = I_m/m$), where m is the mass and I_m the rotational moment of inertia of the bridge deck. The product a_g/ω_g^2 is of unique importance since it measures the excitation's persistency to impose deformation see Dimitrakopoulos et al. [3] and references therein. On the other hand, the latter (ρ) is a length parameter which depends solely on the geometric characteristics of the skew deck (L, W, α) and for a planar skew body it holds: $12\rho^2 = L^2 + W^2/\cos^2\alpha$ [16]. An in-depth analysis of the associated impact [2] shows that the radius of gyration is closely related to the impact response of such structures. Consequently, the response rotation θ max $\rho\omega_g^2/a_g$ is normalized naturally to both a characteristic length scale (a_g/ω_g^2) of the excitation and to a characteristic length scale of the structure's inertial resistance to rotation (ρ), both of which are independent of the response. Similarly, the maximum response displacements, x_m, y_m, and the gap δ are normalized by the persistency of the excitation (terms $x_m\omega_g^2/a_g$, $y_m\omega_g^2/a_g$ and $\delta\omega_g^2/a_g$ respectively), as for pounding and inelastic structures [3].

As Section 3 illustrates the most important feature of the proposed dimensionless terms in Eq. (11) is that they bring forward the remarkable property of self-similarity, a special type of symmetry-invariance which is of unique importance in the non-linear response.

2.3. Overview of the proposed approach

Fig. 4 presents a flowchart of the proposed approach and demonstrates how the different components of this study work together. On one hand, the non-smooth approach introduced in [2] for analysing the oblique impact of skew bridges (impact-LCP in Fig. 4) is extended in order to capture continuous contacts, detachment and transitions between different contact states (detachment-LCP in Fig. 4). On the other hand (Fig. 4-left), the dimensional analysis framework of describing the response of pounding oscillators [1,4] is extended from SDOF structures (pounding structures) to a planar rigid body MDOF structure (skew bridges).

3. The seismic response of a skew bridge subsystem

The seismic response of skew bridges with deck–abutment expansion joints is re-examined adopting the notions of multibody dynamics with unilateral contacts. Before moving on to the seismic response of more realistic bridge models, a bridge subsystem (Fig. 3) is firstly considered. As a first approach, the structural response (apart from contact) is assumed elastic, the restoring characteristics along the two translational directions identical, and no eccentricity (accidental or other, e.g. [16,18]) is considered. Hence, there is no lack of symmetry and the centre of mass coincides with the centre of rigidity where the restoring and inertial properties (the mass and the rotational moment of inertia) are concentrated. Damping is assumed constant for all (translational and rotational) modes of vibration ($\xi = 5\%$).

3.1. Dimensionless description of the seismic response: self-similarity

Fig. 5-left plots the response time histories of the bridge subsystem (Fig. 3) in terms of dimensional displacements [m], for different excitation intensities. The base excitation is a cosine pulse along the x–x axis and the remaining characteristics of the structure and the excitation are presented in Fig. 5(top). Empty circles in the response displacement time histories denote impacts.

When the dimensionless gap $\delta\omega_g^2/a_g$ is fixed, the response curves for different excitation intensities (Fig. 5-left) become self-similar and when expressed in the proposed dimensionless terms (Fig. 5-right) they collapse to a single – master curve (self-similarity). Hence, what is important to the response is not the size of the gap alone (δ), but rather the gap size compared to the persistency of the excitation ($\delta\omega_g^2/a_g$). In previous studies [1,3,4] the property of self-similarity was unveiled for simpler structural configurations of straight bridges; elastic and inelastic structures with (or without) central contact. Herein, the remarkable property of self-similarity emerges even though the response is non-smooth, it involves friction and refers to multiple geometrical directions.

3.2. Rotational response triggered by oblique frictionless contact

Compared with central contact, applicable to straight bridges [4], a major difference in the case of skew bridges, is the coupling of the response among the translational and the rotational degrees of freedom triggered by the oblique contact. With each oblique contact the system is excited in the transverse direction (y–y) and, depending on the geometry of the bridge deck, the rotational degree of freedom may be also excited.

Fig. 6 presents the time history displacements (1st row), rotations (2nd row) and the relative distance (gap functions) of

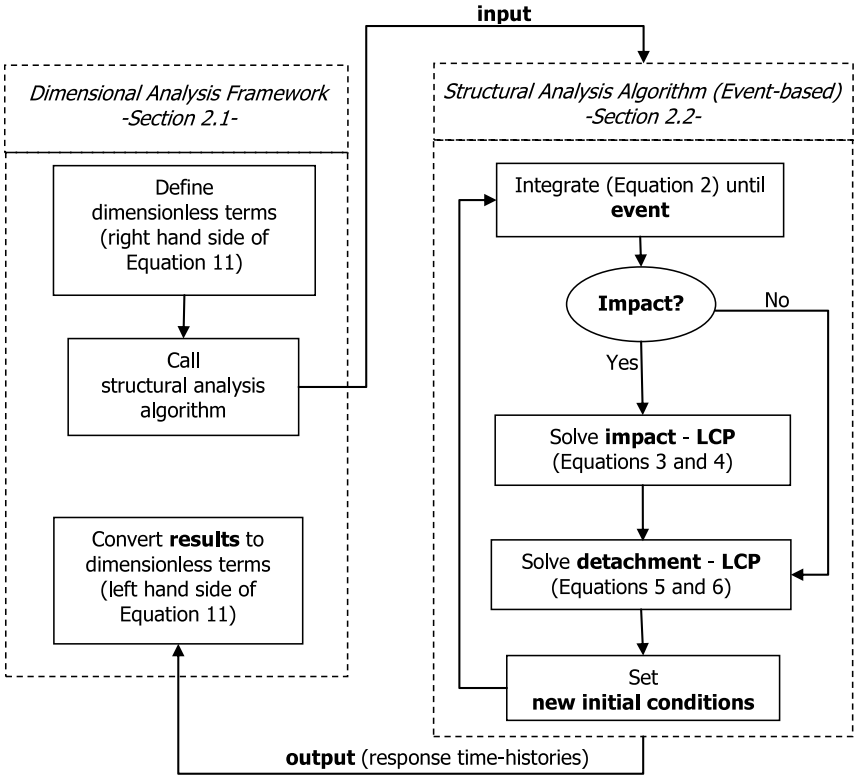

Fig. 4. Flowchart of the proposed approach: The structural response is analysed with an event-based algorithm stemming from non-smooth dynamics (right) and described with the aid of dimensional analysis (left).

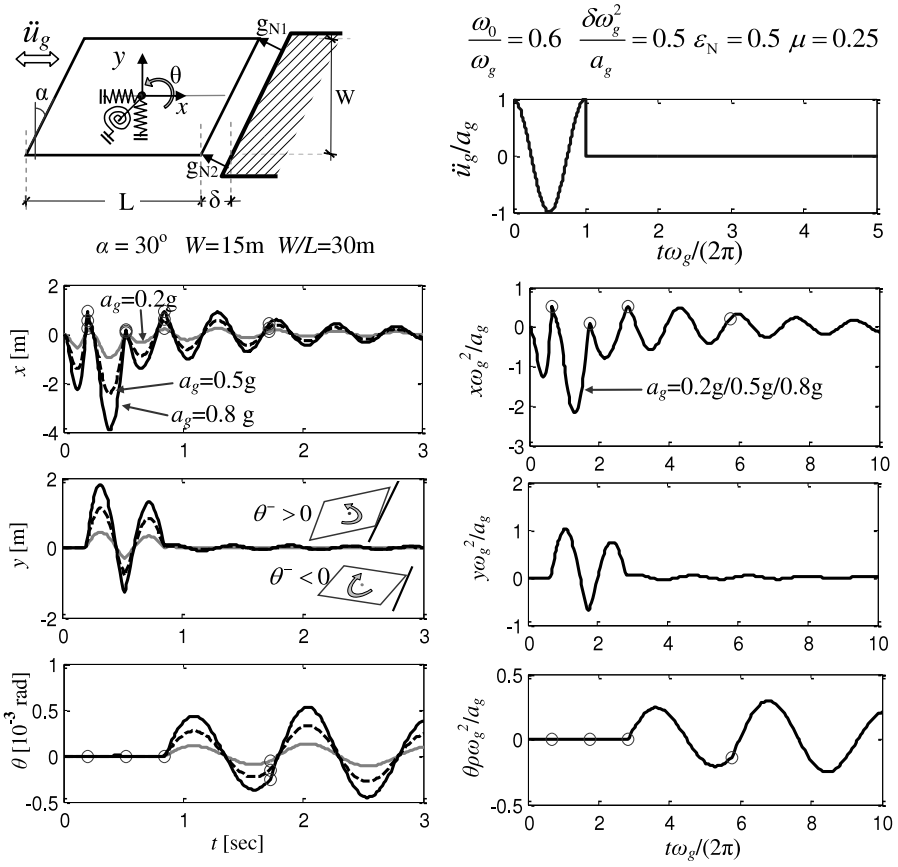

Fig. 5. Left: response time histories: (1st row) relative to the ground displacements along the *x*–*x* axis, (2nd row) along the *y*–*y* axis, and (3rd row) rotations, for different excitation intensities. Right: when the response is described in the proposed dimensionless terms (same results per row), the response curves for different excitation intensities (left) collapse to a single curve (right) (Self-similarity).

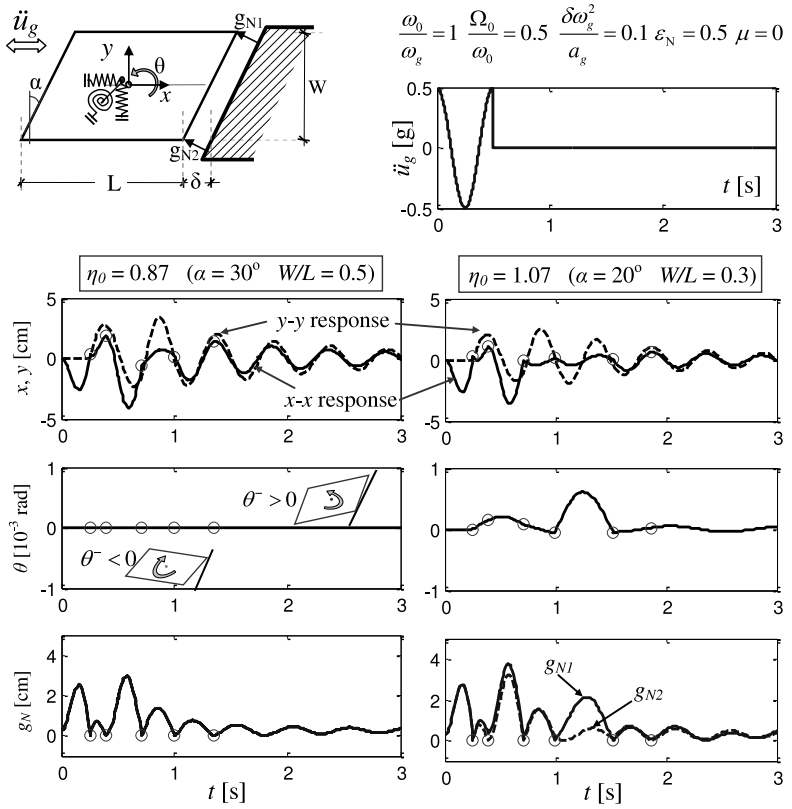

Fig. 6. Seismic response of a skew bridge subsystem for frictionless contact (damping ratio $\xi = 5\%$). Time histories of translational displacements (first row), rotation (second row) and contact distance (third row). Contact results in rotation of the bridge deck, not the for the larger skew angle ($\alpha = 30°$ left) but for the larger dimensionless skew ratio ($\eta_0 > 1$ right).

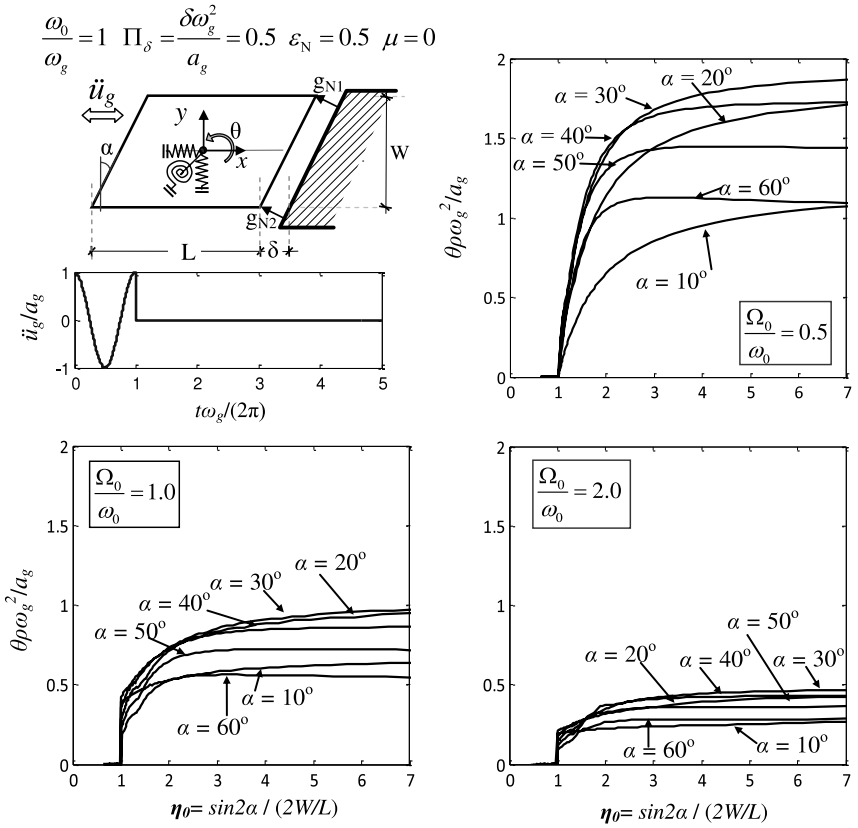

Fig. 7. Maximum dimensionless response rotation $\theta_{max}\rho\omega_g^2/a_g$ versus the dimensionless skew ratio η_0, for different skew angles α and given rotational–translational (Ω_0/ω_0) frequency ratios.

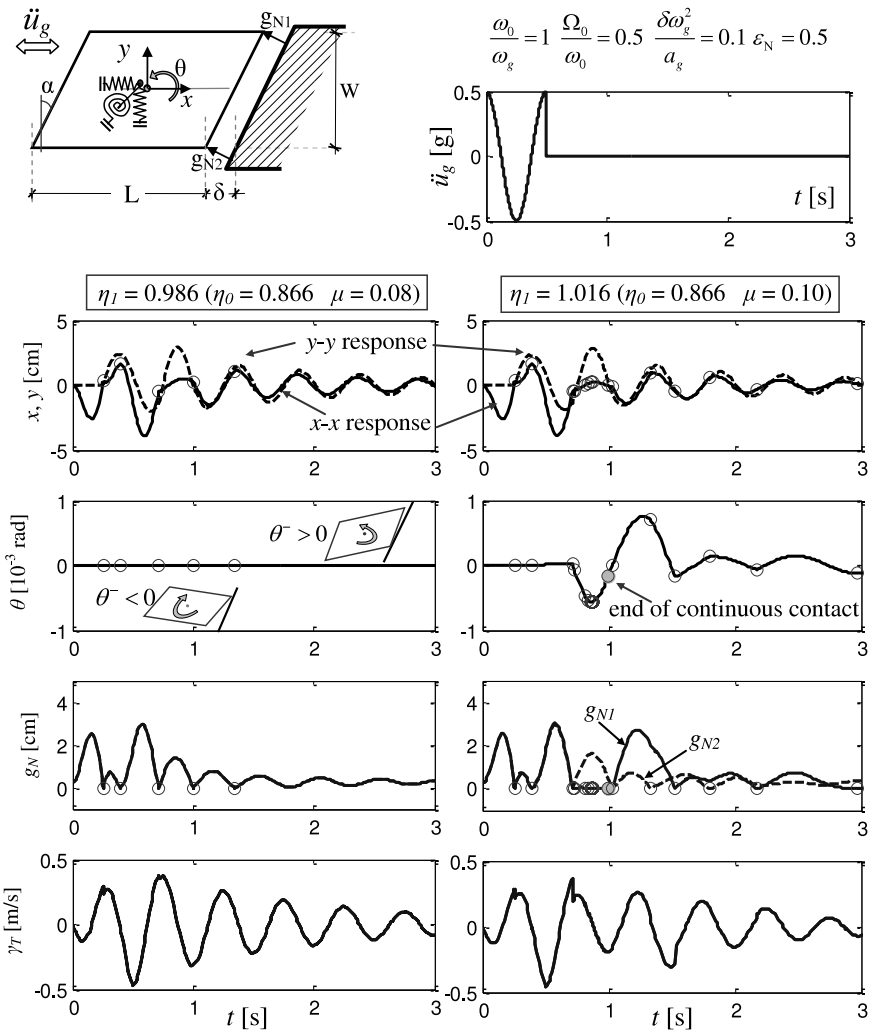

Fig. 8. Seismic response of a skew bridge subsystem for frictional contact (damping ratio $\xi = 5\%$). Time histories of translational displacements (first row), rotation (second row) contact distance (third row) and contact tangential velocity (fourth row).

the two potential contact points g_{N1}, g_{N2} (3rd row) of the skew bridge subsystem of Fig. 3. The system is excited with a cosine pulse (Fig. 6-top right) along the x–x axis and contact is assumed frictionless ($\mu = 0$). Impacts (discontinuous time instants) are denoted with an empty circle, while the end of continuous contacts with filled cycles. Contact takes place either at a corner when $g_{N1} = 0$ or $g_{N2} = 0$ (point contact) or along a side when $g_{N1} = g_{N2} = 0$ (full-edge contact). Since it is assumed that the centre of mass (C.M.) coincides with the centre of rigidity, the response is confined in the direction of the excitation (x–x) until the first (full-edge) contact occurs (Fig. 6).

Depending on the geometry of the bridge deck, the oblique (full-edge)-impact causes the rotation of the deck when the angular momentums of the two impulses are in the same direction with respect to the C.M. (Fig. 2-bottom). Otherwise, contact leads to translational motion without rotation (Fig. 2-top). In order to distinguish these two cases, the dimensionless skew ratio $\eta_0 = \sin 2\alpha/(2W/L)$ was introduced in Dimitrakopoulos [2].

The only difference between the two cases (columns) of Fig. 6 lies in the shape of the bridge deck and hence in the geometry of contact. The remaining characteristics are identical in both cases. The skew segment on the left (Fig. 6) yields a dimensionless skew ratio equal to: $\eta_0 = 0.87 < 1$. Hence [2], despite the numerous (full-edge) contacts (Fig. 6—points where $g_{N1} = g_{N2} = 0$) no rotation is developed throughout the response history. On the other hand, the dimensionless skew ratio in the right column of Fig. 6 is greater than the critical value of unity: $\eta_0 = 1.07 > 1$, as a result the system vibrates in the rotational degree of freedom after the first (full-edge) contact. The relative distance of the two potential contact points g_{N1}, g_{N2} varies and point contacts appear in the remaining time history. In between successive contacts the response in the transverse and the rotational degree of freedom is a free vibration with initial velocities the last post-contact velocities. Consequently, the bridge with the smaller skew angle $\alpha = 20^\circ$ rotates, whereas the bridge with the larger $\alpha = 30^\circ$ does not rotate.

The dependency of the maximum response rotation on the dimensionless skew ratio η_0 is demonstrated in Fig. 7 for given values of the skew angle α. Again, the configuration of Fig. 3 is analysed for a cosine pulse excitation along the x–x axis and results are presented in dimensionless terms. The maximum dimensionless response rotations vary monotonically with the dimensionless skew ratio η_0. Maxima rotations do not scale with the skew angle α, but with the $\sin 2\alpha$ values, i.e. the numerator of the dimensionless skew ratio η_0. This general trend, observed also in the pertinent spectra shown in Figs. 9 and 10, is somewhat different than the early findings of Maragakis [27] which suggested that the response rotation is more sensitive to initial changes in the angle of skew than to changes between 40° and 60°. The response rotation triggered by contact, is very sensitive to small values of the dimensionless skew ratio (say $\eta_0 = 1$–3) and almost

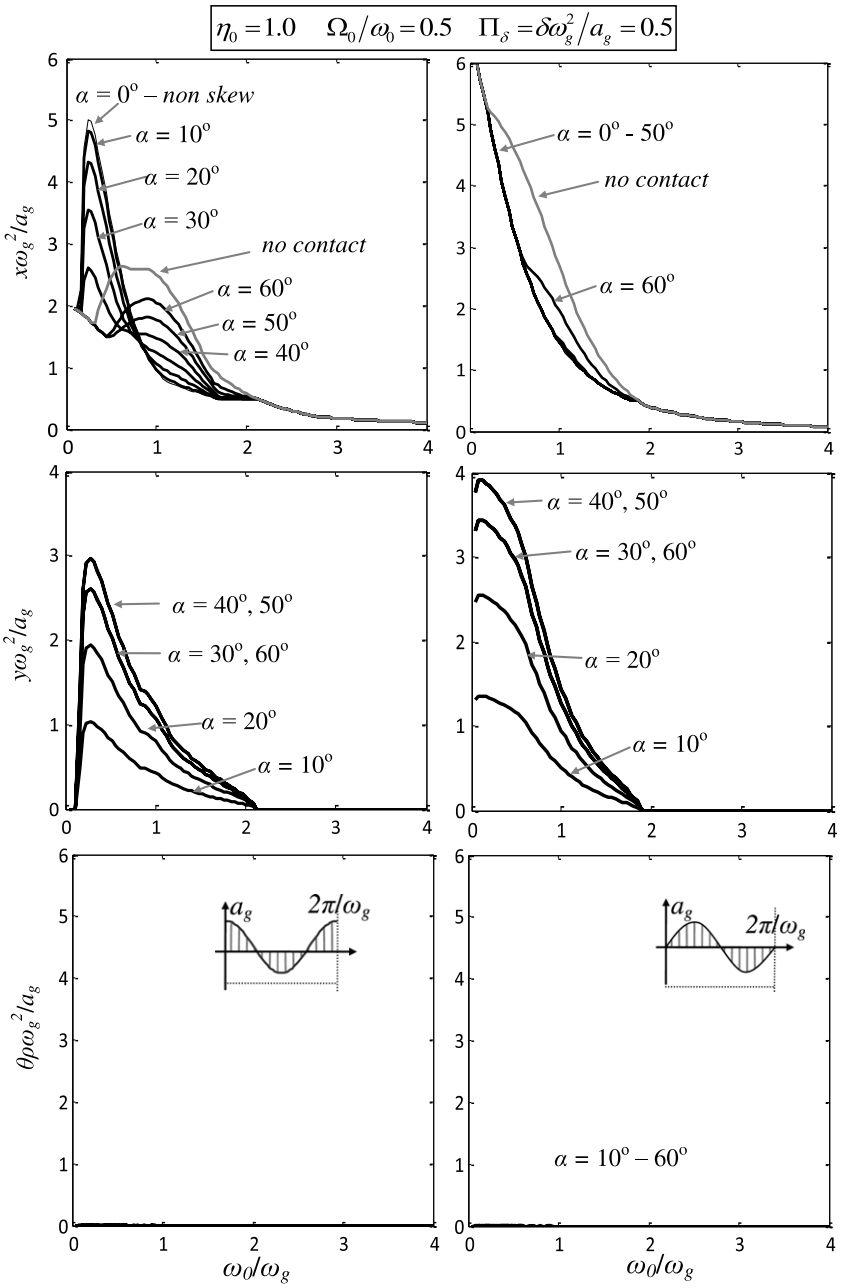

Fig. 9. Self-similar response spectra, in dimensionless terms, of a skew bridge subsystem (Fig. 3) with dimensionless skew ratio $\eta_0 = 1.0$ but different skew angles $\alpha(\varepsilon_N = 0.5, \mu = 0)$. Longitudinal displacements (1st row), transverse displacements (2nd row) and planar rotations (3rd row). Ground excitation: cosine pulse (left column) and sine pulse (right column).

indifferent to values higher than 6, while rotation appears only for η_0 values greater than unity (Fig. 7). This is an important point from a practical point of view, since most skew bridges yield a η_0 value which ranges up to 2. Another, rather straightforward, conclusion drawn from Fig. 7 is that the higher the rotational to translational frequency ratio Ω_0/ω_0 the smaller the response rotations become.

3.3. Rotational response triggered by oblique frictional contact

The seismic behaviour of skew bridges with joints is further complicated by the presence of friction. A frictional contact may lead to slip ($\gamma_T \neq 0$) in one of the two tangential directions of contact or additionally to stick ($\gamma_T = 0$). Frictional contact leads also to sudden changes in the tangential direction of contact velocity which appear as spikes in the velocity time history γ_T (Fig. 8-last row). Frictional contacts may also be instantaneous (impacts) or have a finite duration. In Fig. 8 (right) such a continuous contact is depicted, during which the deck remains in contact (at the acute corner) and slides over the abutment until contact terminates with detachment (filled cycle). These inherent characteristics of non-smooth systems, underline the importance of proper modelling of the deck–abutment, frictional and multi-point, contact in skew bridges.

The rotational mechanism triggered by frictional contact is similar to that of frictionless contact [2], i.e. rotation arises when the angular momentums of the two impulses are in the same direction with respect to the C.M. The pertinent dimensionless ratio for frictional contact reads [2] as: $\eta_1 = \eta_0(1 + \mu/\tan\alpha)$ (Eq. (1)). Fig. 8 plots the response of the mechanical configuration of Fig. 6 (left), under the assumption of frictional contact. The two cases of Fig. 8 differ only in the coefficient of friction, which is $\mu = 0.08$

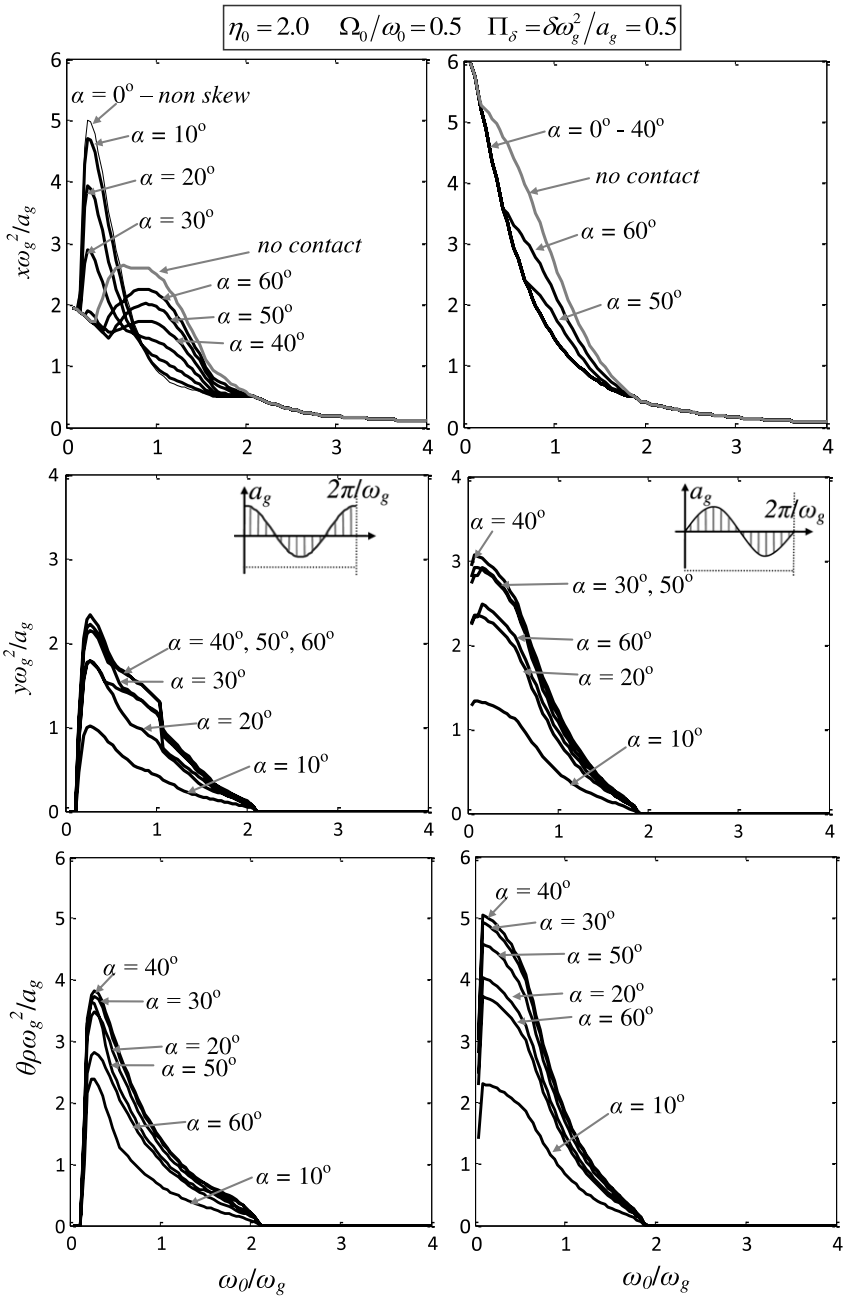

Fig. 10. Self-similar response spectra, in dimensionless terms as in Fig. 9, of a skew bridge subsystem (Fig. 3) with dimensionless skew ratio $\eta_0 = 2.0$ but different skew angles α ($\varepsilon_N = 0.5$, $\mu = 0$).

for the left and $\mu = 0.1$ for the right column respectively. The closely spaced values of friction coefficient in Fig. 8, underline the distinct behaviours around the critical value of the dimensionless skew ratio $\eta_1 = 1$. For a coefficient of friction $\mu = 0.08$ (Fig. 8-left) frictional contact does not yield rotation since the resultant impulses are (marginally) in different directions with respect to the centre of mass ($\eta_1 = 0.99 < 1$) and the angular momentums cancel out [2]. On the contrary, for $\mu = 0.1$ the angular momentums are in the same direction, contact at the acute corner is lost ($\eta_1 = 1.02 > 1$) and the deck rotates after full-edge contact.

3.4. Dimensionless spectra of the coupled response

Figs. 9 and 10 present novel self-similar response spectra of the coupled response of a skew bridge subsystem (Fig. 3). The spectra read in dimensionless terms and are calculated for a given dimensionless skew ratio η_0 but different skew angles α. Fig. 9 differs from Fig. 10 only in the dimensionless skew ratio which is equal to unity $\eta_0 = 1$ (the critical value) and to 2 respectively. Contact is considered frictionless and hence, exactly as for the two cases compared in Fig. 6, rotation appears only for $\eta_0 = 2$, regardless of the frequency of the excitation. Note that for $\alpha = 0$ (no skew) the problem diminishes to the pounding oscillator examined thoroughly in [1] for which no transverse displacements y or rotations θ develop.

In general, even though the response is coupled and quite complex, the shape of the response spectra (Figs. 9–11) of the transverse displacements, as well as the rotations yielded from contact, highlight a clear pattern, to date, unknown. The maximum (contact-induced) transverse displacements (Figs. 9 and 10) as well as the maximum rotations (Fig. 10) both scale with the $\sin 2\alpha$ values ($\sin 20^\circ < \sin 40^\circ < \sin 60^\circ = \sin 120^\circ < \sin 80^\circ = \sin 100^\circ$). This agreement is even better in the absence of rotational response ($\eta_0 \leq 1$). Note that transverse displacements are plotted

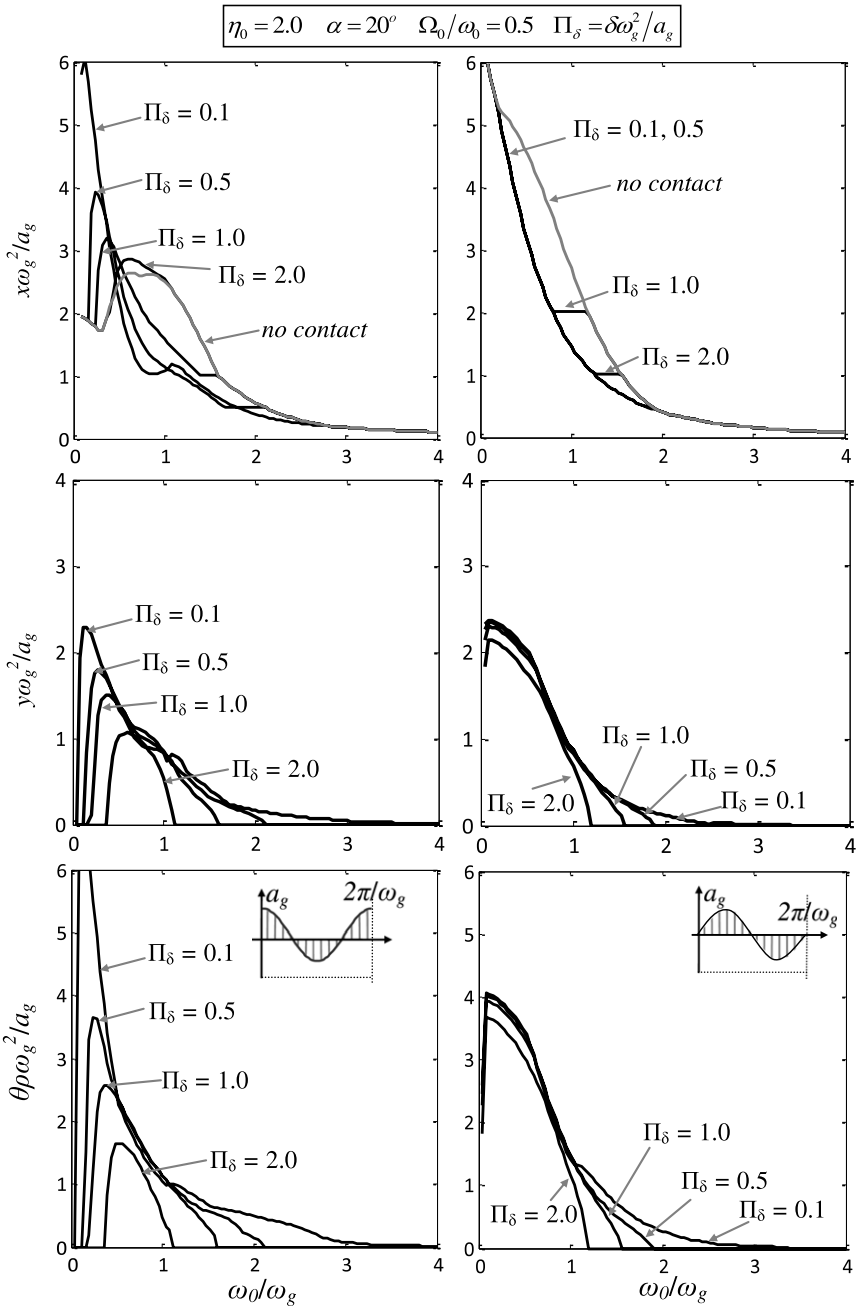

Fig. 11. Self-similar response spectra for a skew bridge subsystem (Fig. 3) with dimensionless skew ratio $\eta_0 = 2.0$ for given dimensionless gaps Π_δ, in dimensionless terms as in Fig. 10.

in a slightly different scale. Furthermore, the influence of contact and hence coupling is more pronounced in the low range of the frequency spectrum (short-period excitations/ flexible structures) and practically negligible in the upper range of the frequency spectrum (long-period excitations/ stiff structures).

On the other hand, the longitudinal response displacement spectra are strongly affected (Figs. 9 and 10) by the skew angle α and they are almost indifferent to the dimensional skew ratio η_0. For small skew angles, say $\alpha = 10^\circ$, the behaviour of the skew bridge subsystem resembles more the response of the pounding oscillator [1] and hence the form of the spectrum is more reminiscent to the pounding oscillator response spectrum. For large skew angles, say $\alpha = 50^\circ$ or 60°, the vibration deviates to the transverse direction, due to contact, and hence the maximum transverse displacements increase. A site-effect of this deflection is that for large skew angles the maximum longitudinal displacements are less sensitive to short-period excitations (low range of the frequency spectrum) and more sensitive to excitations near their natural (translational) frequency. In addition, the differences observed for sine and cosine pulses are similar to those of the response spectra of the pounding oscillator and stem primarily from the very different nature of the two pulses. Sine pulses represent forward motions, while cosine pulses represent forward–backward motions [1].

Fig. 11 investigates the influence of the (dimensionless) gap $\Pi_\delta = \delta\omega g^2/a_g$ size of the coupled response. Self-similar response spectra are offered in dimensionless terms versus the structural to excitation frequency ratio for a fixed skew angle ($\alpha = 20^\circ$).

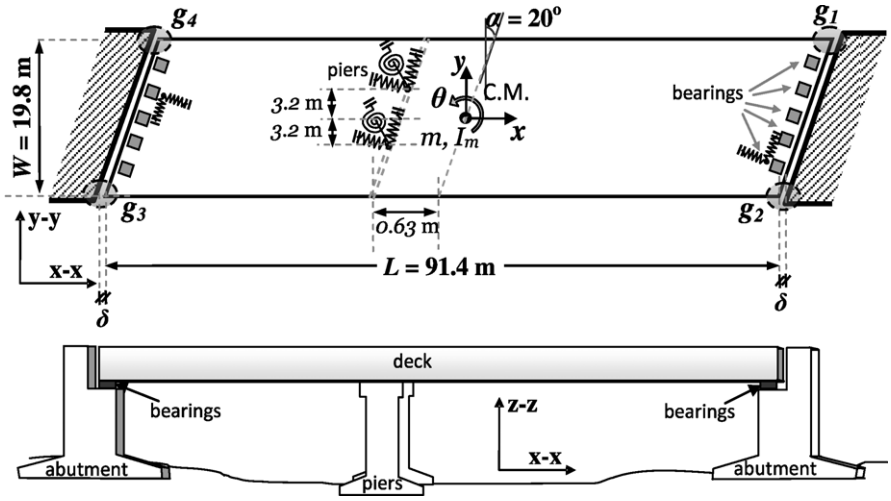

Fig. 12. Model of the bridge examined: plan (top) and elevation (bottom). g_1–g_4 are the potential contact points between the deck (rigid body) and the abutment (inelastic half-space).

The coupling which causes rotations and transverse displacements is more intense for smaller dimensional gaps $\Pi\delta = \delta\omega_g^2/a_g$ and again is maximized in the low range of the frequency spectrum, where contact is more intense and frequent. When both abutments are taken into account though (Section 4), rotations and transverse displacements diminish as the gap size ($\Pi\delta$) decreases.

4. Implementation of the proposed methodology to a skew bridge with deck–abutment joints

The proposed methodology is implemented on a two-span skew bridge with deck–abutment joints. The scope of the application is to estimate the rotations that a (more) realistic bridge model is expected to develop under a wide range of ground motions and investigate how these rotations correlate with the persistency of real ground motions. The examined bridge yields a dimensionless skew ratio equal to $\eta_0 = \sin 2\alpha/(2W/L) = 1.48 > 1$. There are 4 potential contact points (g_1–g_4) shown in Fig. 12 and the contact parameters are estimated as $\varepsilon_N = 0.5$ and $\mu = 0.3$.

The structural configuration illustrated in Fig. 12 is adopted from Maragakis and Jennings [10] with the difference that the abutments are considered as inelastic half-space and the deck–abutment interaction as unilateral contact according to the proposed non-smooth approach. The inertial properties of the bridge model are taken as: $m = 1547$ t and $I_m = 1079\,100$ tm^2 [10]. Both m and I_m are considered concentrated at the centre of mass of the deck. The restoring characteristics of the substructure (piers and bearings) are assumed linear and elastic. The stiffness of each bearing is 34 776 kN/m in both directions, while the stiffness of each pier is 111 199 kN/m in the strong and 81 990 kN/m in the weak axis accordingly. The bridge presents a slight eccentricity: −0.24 m in the x–x, 0.01 m in the y–y direction with respect to the centre of mass (C.M.) while the principal axes are creating an angle of 20° (equal to the skew angle α) with the x–x and y–y axes. The natural frequencies are calculated as: $\omega_{0x} = 18$ rad/s along the x–x axis, $\omega_{0y} = 19$ rad/s along the y–y axis, while the rotational frequency is $\Omega_0 = 26$ rad/s accordingly. Damping is assumed constant for all (translational and rotational) modes of vibration ($\xi = 5\%$).

The system is excited in the longitudinal direction (along x–x axis) with the 62 Greek records considered in [3]. These 62 ground motions comprise most of the available historic Greek records with PGA (peak ground acceleration) of 0.1g or more. In Greece, all types of faults coexist and it should be noted that, intentionally, no shape restriction (pulse-type or otherwise) has been applied for the records examined. The ground motions are characterised using $a_g = PGA$ and $\omega_g = 2\pi/T_m$, where T_m is the mean period [24]. For each record the at-rest size of the joints between the deck and the abutments (δ) is varied, so as to yield a given dimensionless gap term $\Pi\delta = \delta\omega_g^2/a_g$ [3] (Fig. 13: $\Pi\delta = 0.5$-top, $\Pi\delta = 1.0$-middle and $\Pi\delta = 2.0$-bottom).

The results from the 62 records illustrate a satisfying correlation between the persistency of the excitations $L_e = a_g/\omega_g^2$ [m] and the maximum response rotation θ_m (Fig. 13-left). The correlation is better for smaller dimensionless gaps where contact is more frequent. Note that very low rotation values (practically zero) correspond to cases for which contact does not occur and rotation is produced by the slight eccentricity of the bridge. The rotational to translational frequency ratio of the bridge examined is $\Omega_0/\omega_{0x} = 1.43$. Recall that the higher the Ω_0/ω_{0x} ratio, the smaller the response rotations.

For comparison, all excitations are grouped into 4 sets depending on the ratio of the structural frequency to the excitation frequency (ω_{0x}/ω_g). On the right side of Fig. 13 the same response rotations, are offered in dimensionless terms. Unlike the results from the skew bridge substructure (Fig. 11) the rotations of the examined bridge for the smaller dimensionless gap (e.g. $\Pi\delta = 0.5$ Fig. 13) are smaller. This is due to the bilateral obstruction of the rotational vibration, caused by the presence of both abutments. Yet, the rotational response is again more pronounced in the low range of the frequency spectrum where contact phenomena are more intense and/or frequent. In accordance with the proposed spectra (Fig. 11), the dimensionless rotations, arising mainly from contact, decline as the frequency ratios ω_{0x}/ω_g increase and become practically negligible for ω_{0x}/ω_g ratios higher than 2.

5. Conclusions

The aim of the present paper is to bring forward the physical mechanism of the contact-induced coupling in skew bridges with deck–abutment joints. A fully non-smooth rigid body approach is proposed which captures all physically feasible states of single or multi-point frictional contact and impact with linear complementarity formulations.

The seismic response of a simplified skew bridge subsystem to simple pulse ground motions is analysed in depth. The study underlines that the tendency of skew bridges to exhibit transverse displacements and rotate (or potentially unseat) after

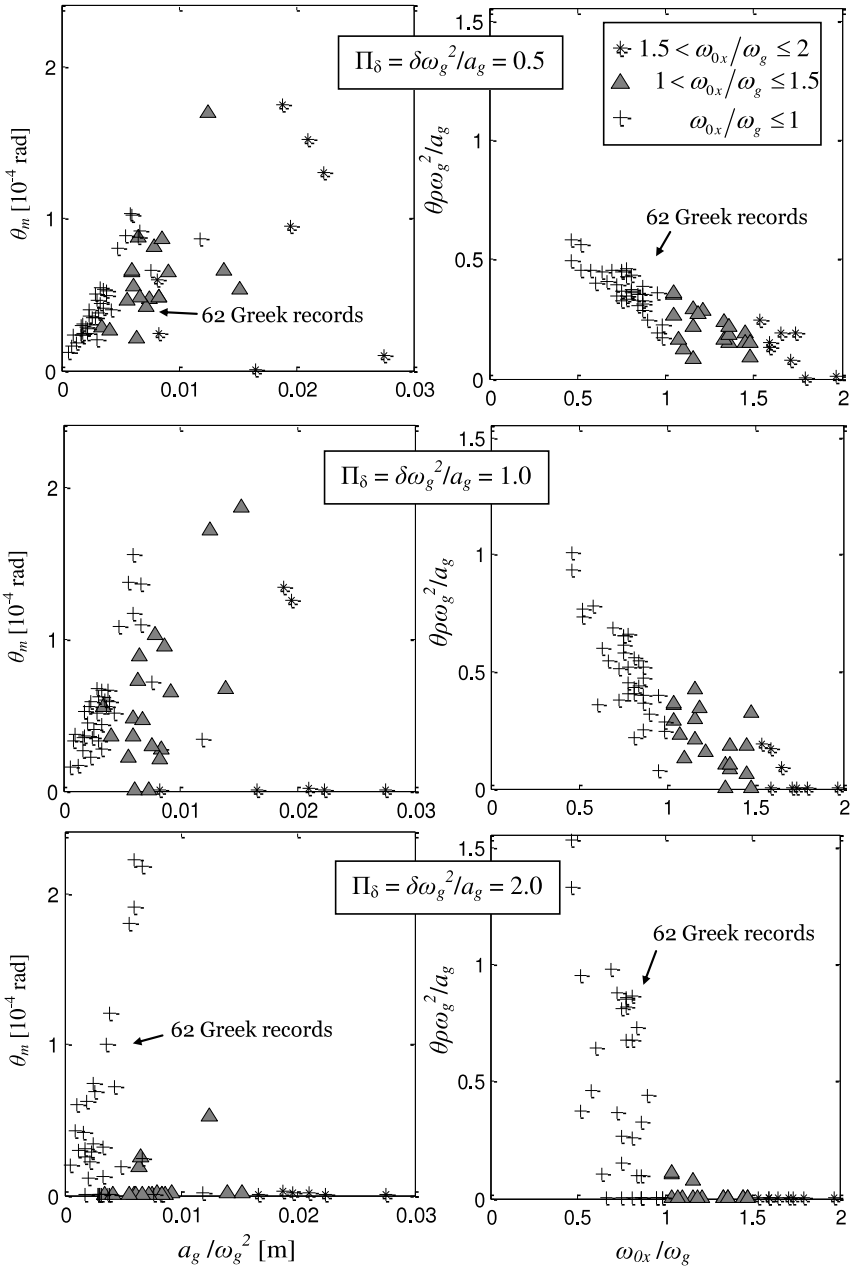

Fig. 13. Seismic response analysis of a skew bridge (of Fig. 12) for given dimensionless gaps. Left: the maximum response rotation θ versus the persistency of the excitation a_g/ω_g^2. Right: dimensionless spectra of the response rotation arising from contact.

deck–abutment collisions is not a factor of the skew angle alone, but rather of the total geometry in plan plus friction. This is expressed with the proposed dimensionless skew ratios η_0 and η_1 for frictional and frictionless contact, respectively. It is shown that the rotational response is very sensitive to small changes of the dimensionless skew ratio η_0 for values just above unity, which correspond to many real-life cases.

Novel self-similar dimensionless response spectra describing the transverse displacements and rotations which arise due to the contact-induced coupling are offered. The proposed spectra of the coupled response (transverse displacements, rotations) scale with the numerator ($\sin 2\alpha$) of the dimensionless skew ratio η_0 and not with the skew angle α. The analysis also unveils that the coupling is more pronounced in the low range of the frequency spectrum (short-period excitations/flexible structures) where contact is more intense and/or frequent.

The applicability of the proposed methodology is illustrated with a pilot application to a typical skew bridge. It is shown that the response rotations arising mainly from contact follow a similar pattern with the proposed spectra and scale well with the persistency of real earthquakes.

Acknowledgements

The present paper is an extension of the doctoral thesis presented by the author to the Civil Engineering Department of the Aristotle University of Thessaloniki. The author gratefully acknowledges the valuable contribution of the supervisors Prof. Andreas Kappos and Prof. Nicos Makris in motivating the ideas presented herein. The revised manuscript has benefited from the valuable comments and suggestions offered by the two anonymous reviewers.

References

[1] Dimitrakopoulos EG, Makris N, Kappos A. J. Dimensional analysis of the earthquake response of a pounding oscillator. J Eng Mech (ASCE) 2010;136(3): 299–310.

[2] Dimitrakopoulos EG. Analysis of a frictional oblique impact observed in skew bridges. Nonlinear Dyn 2010;60:575–95.

[3] Dimitrakopoulos EG, Kappos AJ, Makris N. Dimensional analysis of yielding and pounding structures for records without distinct pulses. Soil Dynam Earthquake Eng 2009;29(7):1170–80.

[4] Dimitrakopoulos EG, Makris N, Kappos AJ. Dimensional analysis of the earthquake-induced pounding between adjacent structures. Earthquake Engng Struct Dyn 2009;38(7):867–86.

[5] Yashinsky M. Performance of highway and railway structures during the February 27, 2010 Maule Chile earthquake, EERI/PEER/FHWA Bridge Team Report. 2010; available online: http://peer.berkeley.edu/publications/chile_2010/reports_chile.html.

[6] Kawashima K, Unjoh S, Hoshikuma J, Kosa K. Damage of transportation facility due to 2010 chile earthquake (April 5, 2010). Bridge Team Dispatched by Japan Society of Civil Engineers. 2010 (available online: http://peer.berkeley.edu/publications/chile_2010/reports_chile.html).

[7] EERL (Earthquake Engineering Research Laboratory). Engineering features of the San Fernando earthquake of February 9, 1971. In: Jennings P.C. editor, California Institute of Technology, Pasadena.

[8] Priestley MJN, Calvi GM, Seible F. Seismic design and retrofit of bridges. Wiley: New York.

[9] FEMA-NIBS. Multi-Hazard Loss Estimation Methodology—HAZUS-MH MR4: Earthquake Model Technical Manual. Developed by the Department of Homeland Security Emergency Preparedness and Response Directorate in FEMA Mitigation Division under a contract with the National Institute of Building Sciences, Federal Emergency Management Agency, Washington, DC; 2003.

[10] Maragakis EA, Jennings PC. Analytical models for the rigid body motions of skew bridges. Earthquake Engng Struct Dyn 1987;15(8):923–44.

[11] Abdel-Mohti A, Pekcan G. Seismic response of skewed RC box-girder bridges. Earthq Eng Eng Vib 2008;7(4):415–26.

[12] Saadeghvaziri M, Yazdanimotlagh A. Seismic behavior and capacity/demand analyses of three multi-span simply supported bridges. Eng Struct 2008;30(1): 54–66.

[13] Bignell J, Lafave J, Hawkins N. Seismic vulnerability assessment of wall pier supported highway bridges using nonlinear pushover analyses. Eng Struct 2005;27(14):2044–63.

[14] Maleki S. Seismic modeling of skewed bridges with elastomeric bearings and side retainers. J Bridge Engrg 2005;10(4):442.

[15] Lou L, Zerva A. Effects of spatially variable ground motions on the seismic response of a skewed, multi-span, RC highway bridge. Soil Dynam Earthquake Eng 2005;25(7–10):729–40.

[16] Meng JY, Lui EM, Liu Y. Dynamic response of skew highway bridges. J Earthquake Eng 2001;5(2):205–23.

[17] Meng JY, Lui EM. Seismic analysis and assessment of a skew highway bridge. Eng Struct 2000;22(11):1433–52.

[18] Meng J, Lui EM. Torsional effects on short-span highway bridges. Comput & Structures 2000;75(6):619–29.

[19] Leine RI, Van Campen DH, Glocker CH. Nonlinear dynamics and modeling of various wooden toys with impact and friction. J Vib Control 2003;9(1–2): 25–78.

[20] Pfeiffer F, Glocker C. Multibody dynamics with unilateral contacts. Weinheim: Wiley-VCH; 2004.

[21] Glocker C. Set-valued force laws: dynamics of non-smooth systems. Berlin (NY): Springer; 2001.

[22] Cottle R, Pang J, Stone RE. The linear complementarity problem. Boston: Academic Press; 1992.

[23] Dimitrakopoulos EG. Analysis of the seismic response of concrete bridges with unilateral contact phenomena, Aristotle University of Thessaloniki (AUTH).

[24] Rathje EM, Abrahamson NA, Bray JD. Simplified frequency content estimates of earthquake ground motions. J Geotech Geoenvir Engrg 1998;124(2):150.

[25] Barenblatt G. Scaling, self-similarity, and intermediate asymptotics. Cambridge (NY): Cambridge University Press; 1996.

[26] Buckingham E. On physically similar systems; illustrations of the use of dimensional equations. Phys Rev 1914;4(4):345–76.

[27] Maragakis EA. A model for the rigid body motions of skew bridges, Report no. EERL 85-02, Caltech, Pasadena CA.